This is a work of the United States Government. In accordance with 17 U.S.C. 105, no copyright protection is available for such works under U.S. Law. Access to this work was provided by the University of Maryland, Baltimore County (UMBC) ScholarWorks@UMBC digital repository on the Maryland Shared Open Access (MD-SOAR) platform.

Please provide feedback

Please support the ScholarWorks@UMBC repository by emailing scholarworks-group@umbc.edu and telling us what having access to this work means to you and why it's important to you. Thank you.

Solar Phys (2019) 294:110
https://doi.org/10.1007/s11207-019-1446-2

The 04 – 10 September 2017 Sun–Earth Connection Events: Solar Flares, Coronal Mass Ejections/Magnetic Clouds, and Geomagnetic Storms

Chin-Chun Wu[1] · **Kan Liou**[2] · **Ronald P. Lepping**[3] · **Lynn Hutting**[1]

Received: 20 November 2018 / Accepted: 20 April 2019 / Published online: 23 August 2019
© This is a U.S. government work and not under copyright protection in the U.S.; foreign copyright protection may apply 2019

Abstract In early September 2017, a series of solar flares and coronal mass ejections (CMEs) erupted from the Sun. The *Cor2a* coronagraph, a unit of the *Sun Earth Connection Coronal and Heliospheric Investigation* (SECCHI), onboard *the Solar Terrestrial Relations Observatory* (STEREO)-A spacecraft recorded two Sun–Earth-directed CMEs on 4 September (referred to as CME04) and 6 September (referred to as CME06). A few days later, the *Wind* spacecraft ($\approx$212.4 solar radii: $R_{\odot}$) recorded two interplanetary shocks, presumably driven by CME04 and CME06, at $\approx$22:41 UT on 06 September 2017 (referred to as Shock06) and at $\approx$22:48 UT on 07 September 2017 (referred to as Shock07), respectively. The travel time of the CME04/Shock06 [$\Delta t_{\text{shock-CME@18R}_{\odot}}$] and CME06/Shock07 from 18 $R_{\odot}$ to the *Wind* spacecraft was 41.52 hours and 32.47 hours, respectively. The propagating speed [V_{CME}] of the CME04 and CME06 at $\approx$18 $R_{\odot}$ was determined with SECCHI/*Cor2a* as $\approx 886\ \text{km}\,\text{s}^{-1}$ and $\approx 1368\ \text{km}\,\text{s}^{-1}$, respectively. Assuming a constant velocity after 18 $R_{\odot}$, the estimated $\Delta t_{\text{shock-CME@18R}_{\odot}}$ is 42.45 and 27.5 hours for CME04 and CME06, respectively. This simple estimate of the CME propagation speed provides a satisfactory result for the CME04 event (error $\approx$2.3%) but not for the CME06 event (error $\approx$15.3%). The second event, CME06, was delayed further due to an interaction with the preceding event (CME04). It is suggested that the CME speed estimated near the Sun with coronagraph images can be a good estimator for the interplanetary CME (ICME) transit time when there is no pre-event. A three-dimensional magnetohydrodynamic simulation is performed to address this issue by providing a panoramic view of the entire process not available from the observations. A southward interplanetary magnetic field [B_s] increased sharply to -31.6 nT on 7 September at *Wind*, followed by a severe geomagnetic storm (Dst $= -124$ nT). The sharp increase of the IMF [B_s] was a result of the interaction between Shock07 and the driver of Shock06 (CME04). This study suggests that a severe geomagnetic storm can be caused by the interaction between a MC, with an impinging IP shock from behind, and the

✉ C.-C. Wu
chin-chun.wu@nrl.navy.mil

[1] Space Science Division, Naval Research Laboratory, Washington, DC 20375, USA

[2] Space Department, Johns Hopkins University, Applied Physics Laboratory, Laurel, MD, USA

[3] University of Maryland Baltimore County, NASA/GSFC, Greenbelt, MD, USA

Earth's magnetosphere. The intensity of a geomagnetic storm will likely be stronger for an event associated with ICME–ICME interaction than for a geomagnetic event caused by only a single ICME.

Keywords Coronal mass ejection · Geomagnetic storm · Interplanetary shock · Interplanetary magnetic field · Space weather prediction · ICME-shock interaction

1. Introduction

Geomagnetic storms belong to the major consequences of space-weather events. In terms of the geomagnetic activity index [Dst] a geomagnetic storm is categorized into three classes: weak (-30 nT $\leq$ Dst < -50 nT), moderate ($-50 \leq$ Dst < -100 nT), and major or severe (Dst ≤ -100 nT) (Gonzalez *et al.*, 1994). Recent studies have established that a coronal mass ejection (CME), a sudden eruption of huge bubbles of coronal material, usually with strong magnetic fields, into the interplanetary medium, is a major contributor to geomagnetic storms (*e.g.* Zhang *et al.*, 2007; Wu *et al.*, 2013). When a CME moves into the solar wind, it becomes an interplanetary structure and is commonly named an interplanetary coronal mass ejection (ICME) (Dryer, 1994). A fast-mode shock may result at the leading edge of the CME/ICME front (*e.g.* Gosling *et al.*, 1975; Sheeley *et al.*, 1985). If any part of the interplanetary (IP) shock arrives at the Earth, this knowledge can be used as a harbinger of geomagnetic activity, because it can compress the magnetosphere and produce the so-called storm sudden commencement (SSC) (Sugiura, 1953). When a geomagnetic storm follows the arrival of an ICME at the Earth, its intensity is weakly dependent on whether or not a shock appears in front of the ICME. Magnetic clouds (MCs) associated with ICMEs and an upstream shock wave tend to produce (three times) larger geomagnetic storms than those without an upstream shock wave (Wu and Lepping, 2016).

It is generally believed that ICMEs and MCs come from the same type of source. Gosling (1990) was the first to report that about 30% of CMEs (now these would be interpreted as ICMEs) appear to contain MCs. Later, various studies show that 41%, 25%, and 28% of ICME were MCs by Bothmer and Schwenn (1996), Cane and Richardson (2003), and Wu and Lepping (2007, 2011), respectively. These results suggest that roughly one-third of CMEs observed near the Earth contain an MC. A large percentage of MCs or ICMEs lead to magnetic storms (*e.g.* Wu and Lepping, 2002a,b; Huttunen *et al.*, 2005). About 90% of MCs were associated with geomagnetic storms (*e.g.* Wu and Lepping, 2002a; Wu, Lepping, and Gopalswamy, 2006). Also, most severe geomagnetic storms are associated with ICMEs or MCs and their driven shocks (*e.g.* Zhang *et al.*, 2007; Wu *et al.*, 2013). These authors attribute their findings to the large, fluctuating magnetic field behind the shock and the large, smooth, and long-duration MC magnetic field (southward) inside the MC that favor magnetic merging. A severe geomagnetic storm has a societal consequence, as it affects space-vehicle operations, interrupts radio communications, and disrupts power grids. Being able to accurately predict the arrival time of IP shocks, driven by ICMEs or MCs, is not only an important scientific subject, but also imperative in space-weather applications.

The propagation speed of ICMEs in the heliosphere can vary significantly, ranging from ≈ 300 to ≈ 1000 km s^{-1} or sometimes much higher at 1 AU (*e.g.* Yashiro *et al.*, 2004; Wood *et al.*, 2017). In other words, it takes, on average, around 18 hours to several days for an ICME to reach the Earth. Observations of CMEs from coronagraphs on the *Solar and Heliospheric Observatory* (SOHO) and/or *Solar Terrestrial Relations Observatory* (STEREO) A/B spacecraft allow us to estimate an ICME's/shock's arrival time at the Earth with a significant lead-time window. Current state-of-the-art shock-prediction models are mainly empirical (*e.g.* Gopalswamy *et al.*, 2000, 2001; Schwenn *et al.*, 2005; Vršnak *et al.*, 2010) or kinematic (*e.g.* Hakamada and Akasofu, 1982; Fry *et al.*, 2001). Although these models are relatively easy to implement and robust, they often provide an averaged prediction uncertainty as large as 10 – 12 hours (*e.g.* Owens and Cargill, 2004).

The "St. Patrick's Day" geomagnetic storm (Dst ≈ -223 nT) on 17 March 2015 was the largest geomagnetic storm in Solar Cycle 24. Using MHD simulations that use the CME propagation speed at 18 $R_\odot$ from coronagraph images, Wu *et al.* (2016a) estimated the CME-driven shock-arrival time at L_1 with a small error (5%). In early September 2017, a series of CMEs erupted from the Sun with two ICMEs propagating toward the Earth. Propagation speed was faster than 1000 $\mathrm{km\,s^{-1}}$ for the CME that erupted on 06 September 2017 (*e.g.* Chashei *et al.*, 2018; Guo *et al.*, 2018). The two ICME events (recorded on 06 September and 07 September 2017) provided us another opportunity to use the measured CME speed at 18 $R_\odot$ [$V_{\mathrm{CME@18R_\odot}}$] to estimate the arrival time of ICME-driven shocks and ICMEs themselves. It motivates us to use the $V_{\mathrm{CME@18R_\odot}}$ to estimate the arrival time at 1 AU and to provide the cause of the severe geomagnetic storm onset on 07 September 2017. Data analysis will be presented in Section 2. A Discussion and Conclusion will be presented in Sections 3 and 4.

2. Observations

2.1. Propagation of CMEs from the Sun to 18 Solar Radii (STEREO Spacecraft)

Figure 1 shows a sequence of white-light coronal images recorded by the *Cor2a* coronagraph, a unit of the *Sun Earth Connection Coronal and Heliospheric Investigation* (SECCHI), onboard the *Solar Terrestrial Relations Observatory* (STEREO)-A spacecraft during 19:24 – 21:54 UT on 04 September 2017. *Cor2a* recorded a CME (named CME04, hereafter) that erupted from the southwest of the solar disk at 19:30 UT (Figure 1b) and appeared as a partial halo CME during 19:30 – 21:54 UT (see Figures 1b – 1f). CME04 was associated with a M1.1 flare that started at ≈ 18:09 UT near S10W11, which was located inside the active region (AR) AR12687. The speed of CME04 is estimated by tracking prominent features, usually at the central front portion of the CME, in time. The slope of the pixel height as a function of time indicates the CME speed and is determined by using least-squares fitting, as shown in Figure 2. The average speed of CME04 is estimated to be 886 $\mathrm{km\,s^{-1}}$.

In less than two days, *Cor2a* recorded another halo CME on 06 September 2017 (named CME06, hereafter). Figure 3 shows a sequence of white-light coronal images during 11:54 – 14:39 UT. CME06 erupted from the southwest (S09W33) of the solar disk at 12:24 UT (Figure 3b, top middle panel) and appeared as a halo CME during 13:24 – 14:39 UT in the field of view (FOV) of *Cor2a*. CME06 was associated with a X9.3 flare that started at ≈ 12:00 UT near S09W33, which was located inside of AR12673. With the same method mentioned in the previous paragraph, the average speed of CME06 is estimated to be ≈ 1368 $\mathrm{km\,s^{-1}}$ (see Figure 4).

2.2. *In-Situ* Observations at L_1 (*Wind* Spacecraft)

Figure 5 shows the *in-situ* solar wind plasma, magnetic field (measured by the *Wind* spacecraft), and the Dst-index during 06 – 09 September 2017 (corresponding to day of year

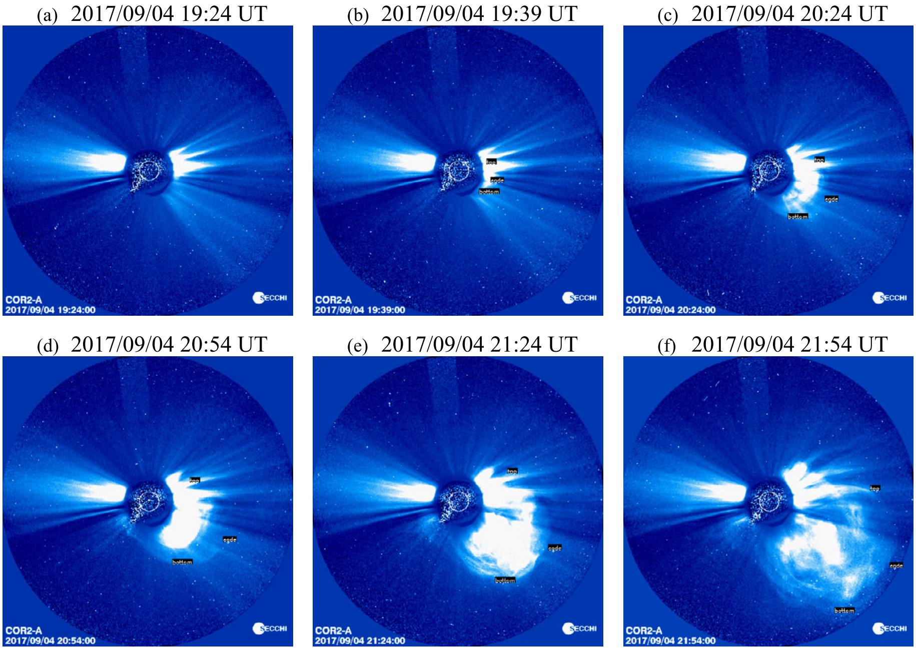

Figure 1 CME images recorded by STEREO/SECCHI *Cor2a* during 19:24 – 21:54 UT (**a**) – (**f**) on 04 September 2017. At 19:39 UT (**b**) *Cor2a* recorded a CME that erupted near the solar Equator.

Figure 2 Propagation speed of the CME on 04 September 2017: the average speed at the middle (center) of the CME is 886 km s^{-1}.

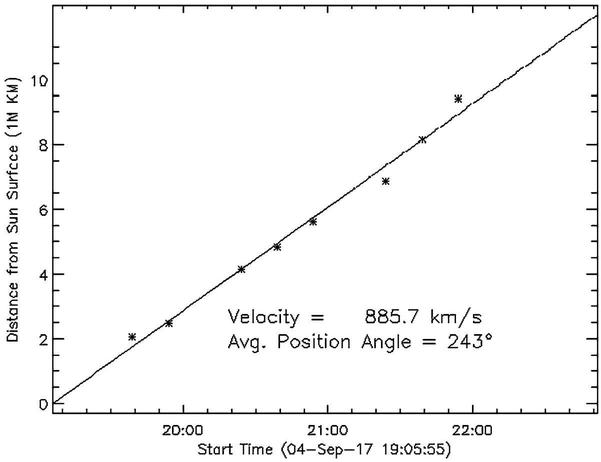

(DOY) range = 249 – 252). The *Wind* spacecraft was located at approximately 213 solar radii [R$_{\odot}$] from the Sun during that period. *Wind* recorded two IP shocks: one at ≈ 22:41 UT on 06 September 2017 (named Shock06, hereafter) and the other at ≈ 22:48 UT on 07 September 2017 (named Shock07, hereafter), respectively.

An SSC occurred at 23:00 UT on 06 September 2017 within one hour after the passage of Shock06 measured by the *Wind* spacecraft. After Shock06 encountered the *Wind* spacecraft, Dst increased continuously, and it peaked at ≈ 51 nT at 02 UT. After that, the value of

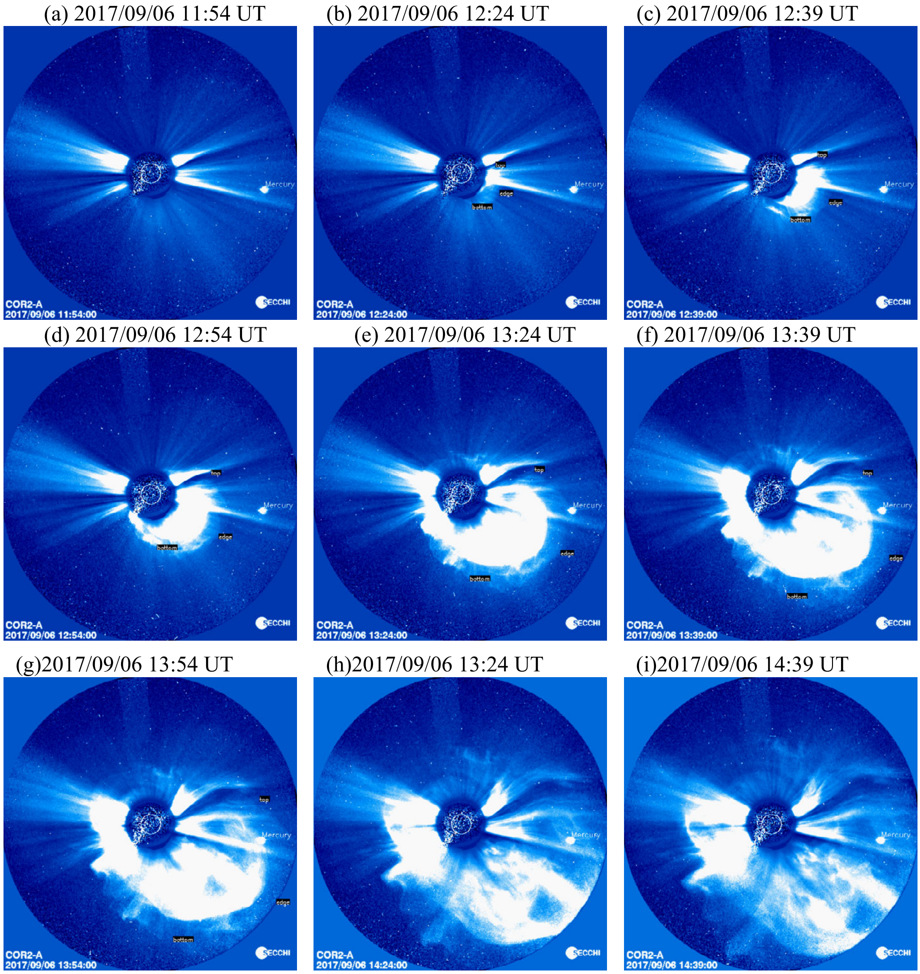

Figure 3 CME images recorded by STEREO/SECCHI *Cor2a* during 11:54 – 14:39 UT (**a**) – (**i**) on 06 September 2017. At 12:24 UT (**b**) *Cor2a* recorded a CME that erupted near the solar Equator.

Dst started decreasing immediately after the IMF turned southward (see Figure 5g) and dropped to −3 nT at 11 UT. Then the Dst stayed (or hovered) around zero for many hours, presumably in response to the sheath field (Sheath06). At ≈ 18 UT on 7 September, a MC (referred to as MC07, hereafter) encountered the *Wind* spacecraft and lasted for ≈ 7.25 hours (*i.e.* MC07 ended at 01:52 UT on 08 September 2017). An IP shock was recorded inside MC07 at ≈ 22:25 UT on 07 September 2017 (DOY 250.934).

This IP shock is referred as Shock07, hereafter. Shock07 was associated with a sharp (further) drop in the IMF B_z-component, which reached −31.6 nT. The sharp drop in B_z induced a sharp Dst drop to −124 nT at 02 UT on 8 September. This large geomagnetic storm was associated with the southward magnetic field inside of MC07. We refer to this geomagnetic storm as Storm07.

After Dst dropped to its minimum value of −124 nT at 02 UT on 08 September, Storm07 started to recover and lasted for ≈ 8 hours. At 10:00 UT on 08 September 2017 an MC-

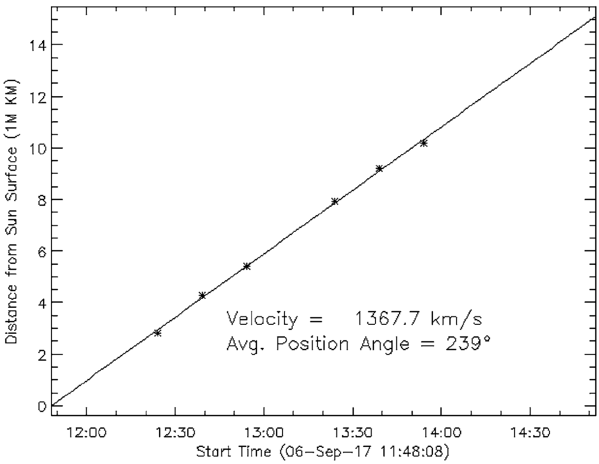

Figure 4 Propagation speed of the CME on 06 September 2017: The average speed at the middle (center) of the CME is 1368 $\mathrm{km\,s^{-1}}$.

like structure (named MC08, hereafter) was observed by *Wind*, and the IMF B_z-component showed a sharp, southward turning and reached a minimum value of −13 nT. Then Dst dropped to −109 nT at 1800 UT on 08 September 2017. The duration of MC08 (which was the driver of Shock07) was ≈ 7 hours.

3. Discussion

3.1. Estimation of Shock-Arrival Time at 1 AU

Table 1 summarizes relevant information about CME04, CME06, Shock06, and Shock07. For example, the arrival times for the leading edges of CME04 and CME06 at 18 $R_\odot$ were ≈ 20:00 UT 04 September 2017 and ≈ 12:24 UT 06 September 2017, respectively, as derived from Figures 2 and 4. From the time difference, the propagation time of the CME-driven shock [$\Delta t_{\text{shock-CME@18R}\odot}$] from 18 $R_\odot$ to *Wind* was 41.5 hours for CME04 and 32.5 hours for CME06 (the actual propagation time depends on which part of the associated ICME reached *Wind*). This time difference will be used as the ground truth. Here we test if the CME propagation time can be estimated reasonably using the CME speed measured with the STEREO/SECCHI *Cor2a* coronal images. $V_{\text{CME/shock}}$ is 886 $\mathrm{km\,s^{-1}}$ for CME04, and it is 1369 $\mathrm{km\,s^{-1}}$ for CME06. Assuming a constant propagation speed, the travel time is simply the propagation distance divided by the average propagation speed. This gives 42.4 and 27.5 hours for CME04 and CME06, respectively. While simple, this estimation provides satisfactory agreement for the CME04–Shock06 event. Therefore, it is suggested that $V_{\text{CME@18R}\odot}$ (estimated by using *Cor2*'s coronagraph images) can be a good estimator for the CME-driven shock's arrival time (SAT) at the Earth when there is no pre-event. Note that this method has been used previously by Wu *et al.* (2016a) for the 15 March 2015 event (referred to as CME15), with an error of ≈ 5%. On the other hand, this simple ballistic method fails for the CME06 event. It is found that the predicted time is longer than the actual propagation time by ≈ 15.3%. This suggests that the assumption of a constant propagation is not correct for the CME06 event and for this particular event. We suggest the following two possibilities to explain this: i) the CME06–Shock07 event is farther away from the Sun–Earth line than the other two events (CME04 and CME15); and ii) ICME–ICME interactions possibly occurred.

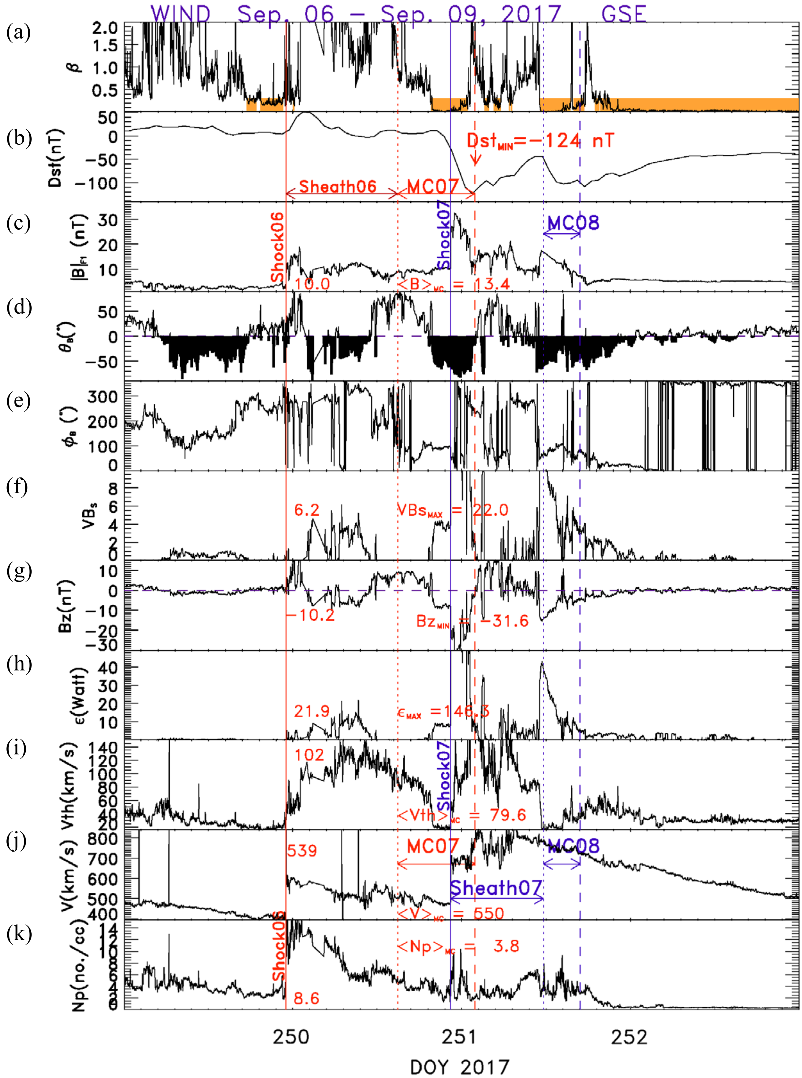

Figure 5 Geomagnetic activity index (Dst: **panel b**) and *Wind*-observed *in-situ* solar wind parameters 06 – 10 September 2017. *From top to bottom*: (**a**) proton plasma beta, (**b**) Dst, (**c**) magnetic field [B] in terms of magnitude, (**d**) – (**e**) latitude [θ_B], and longitude [ϕ_B] in GSE coordinates, (**f**) induced magnetic field [VB_S], (**g**) B_Z of the field in GSE, (**h**) Akasofu ϵ, (**i**) thermal velocity [V_{th}] or proton temperature [T], (**j**) bulk speed [V], and (**k**) number density [Np]. The *blue horizontal line* in **panel c** represents the scheme's identification of the extent of this MC candidate (Lepping, Jones, and Burlaga, 1990). The *purple-solid line* and *blue-dashed vertical lines* represent the IP shock and the front boundary of the MC.

Now we consider the first possibility. The source locations of CME04, CME06, and CME15 were S10W11, and S10W33, and S22W25, respectively. Earth was orbiting around N7.2° during 4 – 6 September 2017, and around S7.2° on 15 March 2015. Mapping the Earth to the surface of the Sun, the angle between the center of Sun and the source location of the CME (referred as $\text{Sun}_{\text{center}}$–CME-line), the angles for the center of the Sun to the Earth (re-

Table 1 Related information for the CME04/06, Shock06/07 during 04 – 09 September 2017.

	CME04	CME06
Start time	04 September 2017 19:39 UT	06 September 2017 12:24 UT
End time CME$_{@18R_\odot}$	04 September 2017 23:10 UT	06 September 2017 14:20 UT
Shock$_{@Wind}$	07 September 2017 22:41 UT (Shock06)	07 September 2017 22:48 UT (Shock07)
[a] $V_{\mathrm{CME/shock}@18R_\odot}$ [km s^{-1}]	866	1368
[b] Δr [R$_\odot$]	194.84	194.84
[c] $\Delta t_{\mathrm{Shock\text{-}CME}@18R_\odot}$ [hours]	47.52	32.47
[d] Δt_{pred} [hours]	43.47	27.52
[e] $\Delta t_{\mathrm{Error}}$ [hours]	4.05	4.97
[f] Error [%]	8.5	15.3
[g] $\langle V_{\mathrm{shock}}\rangle$ [km s^{-1}]	792	1159

[a] $V_{\mathrm{CME/shock}@18R_\odot}$: measured by using SECCHI-*Cor2a* (see Figures 2 and 4) [km s^{-1}].

[b] Δr [R$_\odot$] = Distance between 18 R$_\odot$ and *Wind* spacecraft: Location of *Wind* [212.839 R$_\odot$] – inner boundary of G3DMHD (18 R$_\odot$) = 194.839 R$_\odot$; units are in solar radii [R$_\odot$ = 695,500 km].

[c] $\Delta t_{\mathrm{shock\text{-}CME}@18R_\odot}$: observed travel time of CME/shock from 18 R$_\odot$ to the *Wind* spacecraft [hours].

[d] Δt_{pred}: $\Delta r / V_{\mathrm{CME/shock}@18R_\odot}$ [hours].

[e] $\Delta t_{\mathrm{Error}} = |\Delta t_{\mathrm{pred}} - \Delta t_{\mathrm{OBS}}|$ [hours].

[f] Error $= |\Delta t_{\mathrm{pred}} - \Delta t_{\mathrm{OBS}}|/\Delta t_{\mathrm{OBS}} \times 100$ [%].

[g] $\langle V_{\mathrm{shock}}\rangle = \Delta r/\Delta t_{\mathrm{Shock\text{-}CME}@18R_\odot}$: averaged propagating speed of an IP shock from 18 R$_\odot$ to *Wind*.

ferred to as Sun$_{\mathrm{center}}$–Earth line) are 20.39°, 28.28°, and 37.09° for CME04, CME15, and CME06, respectively. Therefore the source of CME04 was located closest to the Sun$_{\mathrm{center}}$–Earth line, followed by CME 15 and then CME 06. This suggests that distance between the CME's source location and the Sun$_{\mathrm{center}}$–Earth line could play an important role on the accuracy of the forecast for SAT. Note that an event where there is a shock inside a MC is very complicated and fairly rare. Less than ten such events were identified from the *Wind* data during the past 23 years (1995 – 2017). Further studies are required to assess the probability quantitatively. This is beyond the scope of this study.

3.2. What Caused the Severe Storm in September 2017?

A geomagnetic storm can be induced by a southward IMF in the MC sheath, the leading (*i.e.* front part) region of a MC, the trailing part of an MC, and both sheath and MC regions (*e.g.* Wu and Lepping, 2002a). During early September 2017, two IP shocks (Shock06, Shock07) and two MCs (MC07, MC08) were identified (see Figure 5). MC07 and MC08 were the drivers for IP Shock06 and Shock07, respectively (see details in Section 3.1). MC07 and MC08 were identified by two procedures: i) we first applied the automatic MC auto-identification (MCI) routine (Lepping, Wu, and Berdichevsky, 2005) to find the MC candidate, and then ii) we used a MC-fitting (MCF) model (Lepping, Jones, and Burlaga, 1990) to determine the MC parameter values, and to be sure that the structure is a *bona fide* MC. Figures 6a and 6b show MC17's magnetic-field structure in cloud coordinates and GSE coordinates, respectively. The solid-black curves are the MC-fitting results. Figure 6 shows that the MCF model is capable of fitting the MC obscurations including a dynamically evolving structure (shock), as far as field direction is concerned, but the field magnitude

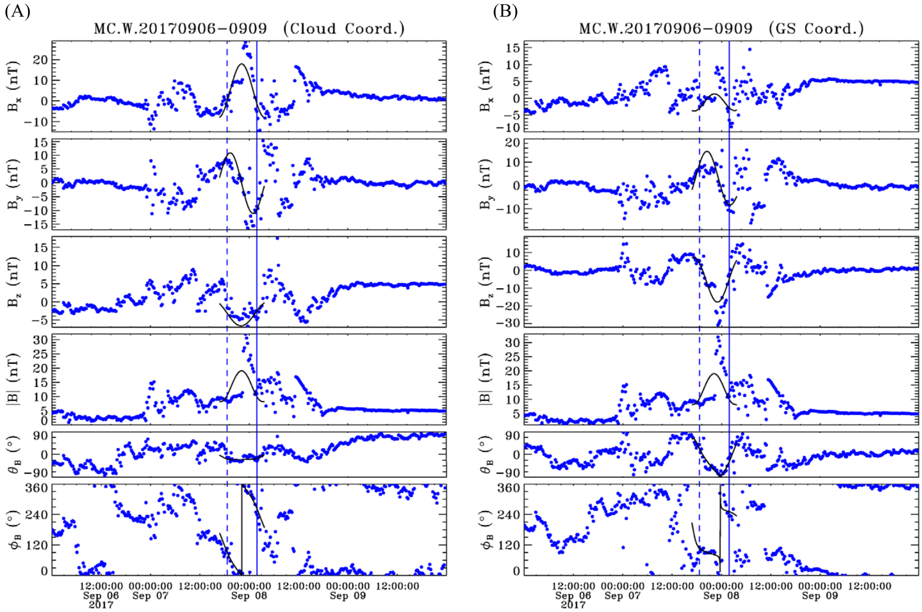

Figure 6 The MC of 07 September 2017. This is a poor-quality ($Q_O = 3$) example of the use of the Lepping, Jones, and Burlaga (1990) MC-fitting model where the points are the observed magnetic-field data (in 15-minute average form), and the *solid black curves* are the result of the model, and Q_O is defined by Lepping *et al.* (2006). The *blue-dotted curves* represent *in-situ* observations at L_1 (*Wind*). (**A**) The *left six panels* are given in cloud coordinates (CL, Lepping *et al.*, 2006) in terms of magnetic field in x-, y-, z-components [B_X, B_Y, B_Z], field intensity [$|B|$], latitude [θ_B], and longitude [ϕ_B], and (**B**) the *right six panels*, for the same physical quantities, are in geocentric-solar-ecliptic [GSE] as designated. The *dashed vertical line* is the estimated MC start time (see Table 2), and the *solid vertical line* is the estimated end-time. Note that "GS Coord." *on the top* of (**B**) means GSE coordinate.

is not well modeled, especially when the internal shock occurs. However, field magnitude is well modeled, on average. This is true in general, not just for this case. A sheath is the region between a shock and a MC. Sheath06 was named for the region between Shock06 and MC07, and Sheath07 was named for the region between Shock07 and MC08. Note that MC07 (which started at 19:44 UT on 07 September) was about 21 hours behind Shock06 (which started at 22:41 UT on 06 September). It is reasonable to assume that MC07 was the driver of Shock06, because past statistical results show that the duration of a sheath (the area between a shock and an MC) is usually in the range of 1 – 28 hours (see Figure 1b of Wu and Lepping, 2016). Therefore, it is not unreasonable to assume that MC07 is the driver of Shock06. Also, if the direction of the spacecraft's velocity is significantly displaced from the shock's normal at its nose, the sheath-duration can become quite large, as shown by Wu and Lepping (2016).

Storm07 is a complicated storm, because $B_{z\text{-min}}$ was caused by the interaction of Shock07 that ran into MC07. Storm07 was caused by the southward IMF B_z in the regions of Sheath06, MC07, and Sheath07. Therefore, Storm07 can be cataloged as a two-step storm (Sheath06+MC07) or a sheath storm (Sheath07). Figure 5 shows that Dst dropped dramatically at the time associated with the rear part of MC07. The sharp decrease of $B_{z\text{-min}}$ was caused by the interaction between MC07 and Shock07. Here, we conclude that Storm07 was a product of an interaction between MC07 and shock07, because the sharp decrease of Bz_{min} was caused by the interaction between MC07 and Shock07.

Table 2 The MC fit-parameters for the MC that occurred on 7 September 2017 (starting day).

Starting time = 18:37 UT	CA [%] = −3%
$\Delta T = 7.25$ hours	$\Delta t = 15$ minutes
$V_{MC} = 550\ \mathrm{km\,s^{-1}}$	$\beta_{CA} = 4.3°$
$2R_o = 0.0999$ AU	Check = 3.9%
$B_o = 20.22$ nT	$\Phi_o = 1.29 \times 10^{20}$ Mx
$H = +1$ right-handed	$J_o = 5.7\ \mu\mathrm{A\,km^{-2}}$
$\theta_A = -52°$ and $\phi_A = 48°$ (GSE coordinates)	$I_T = 3.9 \times 10^8$ Å
$\chi_R = 0.244$	$N = 30$
Asf [%] = 1.8%	$Q_o = 3$

*Definitions of Magnetic Cloud Quantities.

ΔT: Duration of the MC encounter (*i.e.* ΔT = end time – start time of MC passage).

V_{MC}: Average solar wind speed [$\mathrm{km\,s^{-1}}$] within the MC.

$2R_o$: Estimated diameter [AU], where R_o is the model-estimated radius.

B_o: Estimated axial magnetic-field magnitude [nT].

H: Handedness (+1 for right-handed or −1 for left-handed).

ϕ_A, θ_A: Longitude and latitude, respectively, of the MC-axis (GSE coordinates).

t_o: Estimated center-time of the MC.

χ_R: Square root of the reduced chi-squared of the MC fit.

asf [%]: Asymmetry factor [%], which depends on t_o and ΔT.

CA [%]: Estimated relative closest approach distance, *i.e.* y_o/R_o [%] where y_o is closest approach.

Φ_o: Estimated axial magnetic flux [10^{20} Mx].

J_o: Estimated total axial current density [$\mu\mathrm{A\,km^{-2}}$].

Δt: Length of the averages used in the analysis; these are usually 15 minutes, 30 minutes, or 1 hour.

β_{CA}: Cone angle, the angle between the MC-axis and the X-axis [GSE coordinates].

Check: A check of the estimated radius by using duration, speed, CA, cone angle, and R_o.

I_T: Estimated total axial current [10^8 A].

N: Number of points used in the MC-fitting interval.

Q_o: Estimated quality of the model fitting (where $Q_o = 1, 2$, or 3, for excellent, good, or poor, respectively); see Lepping *et al.* (2006).

It is not typical for an IP shock to be observed in the rear part of a MC. According to Collier, Lepping, and Berdichevsky (2007), only 6 MC–Shock interaction events (out of 82 MCs) were reported in the early era of the *Wind* mission, *i.e.* from November 1994 through August 2003. These six MC–Shock events occurred on 19 October 1995, 07 November 1997, 25 June 1998, 20 March 2002, 25 March 2002, and 18 June 2003. MC's IMF rotated from South to North (S–N) for the events on 19 October 1995, 07 November 1997, 25 June 1998, and 25 March 2002; and North to South (N–S) for the events on 20 March 2002 and 18 June 2003. For the event on 20 March 2002, B_z was northward in the very early part of the MC, and southward B_z was weak in the rear part of MC. This event caused only weak geomagnetic activity.

For the event on 18 June 2003, an IP shock (referred to as Shock18) encounter at the rear part (about three-fourths of the way in) of the MC. B_z was ≈ -5 nT and −18.4 up- and down-stream of Shock18. Dst was in a range between −20 and −50 nT in the early part of the MC. Dst decreased to −145 nT at the time of the downstream of Shock18 (see Figure 7).

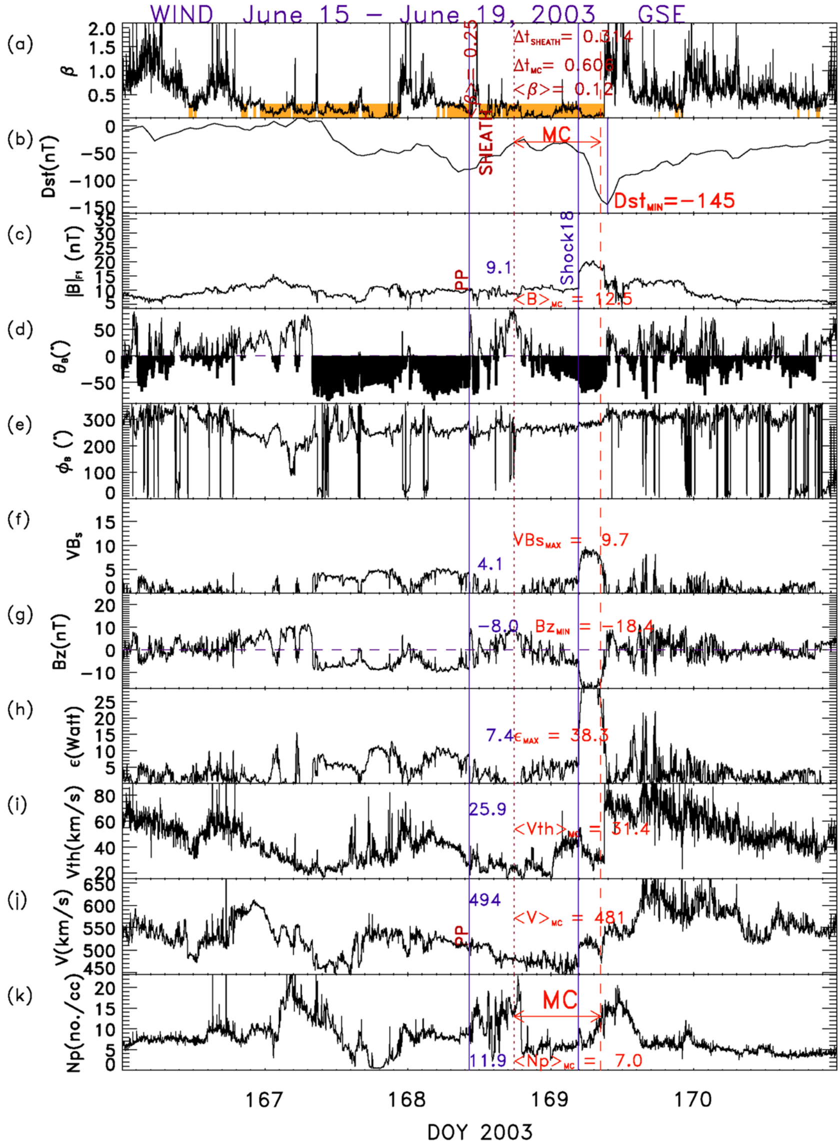

Figure 7 Geomagnetic activity index (Dst: *second panel*) and *Wind*-observed *in-situ* solar wind parameters 15 – 19 June 2002. From *top to bottom*: proton β, Dst, $|B|$ field magnitude, latitude [θ_{B}], and longitude [ϕ_{B}] in GSE coords., VB_{S}, B_{Z} of the field in GSE, proton thermal speed [V_{th}], bulk speed [V], and number density [Np]. The *vertical blue-solid line* and *blue-dashed lines* represent the IP shock and the front boundary of the MC.

According to the study of Collier, Lepping, and Berdichevsky (2007), Shock18 was driven by a halo CME ($V_{\mathrm{CME}} = 2053\ \mathrm{km\,s^{-1}}$), which erupted at $\approx$23.9 hours on 15 June 2003, and the associated source location of the presumably associated flare was S20W81. Again, the MC–Shock event on 18 June 2003 confirmed the finding of this study: the storm can be enhanced by shock compression of B_{z} inside the MC.

A large southward IMF can be associated with various kinds of solar wind structures: i) an interplanetary (IP) shock wave (sheath) (*e.g.* Tsurutani *et al.*, 1988; Kamide *et al.*, 1998; Wu and Lepping, 2008, 2016), ii) part of a magnetic cloud (MC) (*e.g.* Wu and Lepping, 2002a, 2002b) or an IP coronal mass ejection (ICME) (*e.g.* Richardson and Cane, 2011; Wu and Lepping, 2011), iii) a heliospheric-current-sheet sector boundary crossing (*e.g.* McAllister and Crooker, 1997), or iv) a combination of these interplanetary structures (*e.g.* Tsurutani and Gonzalez, 1997; Echer and Gonzalez, 2004). We study a new category of storm type: MC–Shock interaction. The severe storm that occurred during 07 – 08 September 2017 was produced by such an interaction.

3.3. An MHD Simulation to Validate V_{CME} in the Plane-of-the-Sky Used for CME Propagation

One may argue that the accuracy of the above prediction of the shock-arrival time at the Earth (SAT) is poor because the technique used to measure the CME speed is not the true CME speed but the plane-of-the-sky speed and can be subjective. We have many years' of experience in measuring V_{CME} with coronagraphs and in studying CMEs' associated solar wind structures at the Earth (*e.g.* Wood *et al.*, 2011, 2012, 2017; Wu *et al.*, 2011, 2016b,c, 2017). Based on our previous work, we believe that the technique generally provides reasonably accurate initial CME speeds. As a double check, we perform a global three-dimensional (3D) magnetohydrodynamic (MHD) numerical simulation. The simulation is done with a well-developed H3DMHD model (Wu *et al.*, 2007a,b, 2016a,b), which is capable of simulating realistic time series of solar wind profiles at the Earth. The H3DMHD model uses the HAF model (Fry *et al.*, 2001) to generate solar wind parameters at the inner boundary of the heliosphere in order to drive the 3DMHD model that was originally developed by Han, Wu, and Dryer (1988). In this study, we will use our newly developed scheme to replace the HAF model, which is not conveniently available for the present study. The new scheme provides the relationship between the expansion factor and solar wind speed at 18 $\mathrm{R}_{\odot}$ (Wu *et al.*, 2019).

The 3DMHD model solves a set of ideal-MHD equations using an extension scheme of the two-step Lax–Wendroff finite difference method (Lax and Wendroff, 1960). The induction equation is used to take into account the nonlinear interaction between the plasma flow and the magnetic field. The computational domain for the 3D MHD simulation is a Sun-centered spherical coordinate system (r, θ, ϕ) oriented on the Ecliptic plane. The Earth is located at $r = 215\ \mathrm{R}_{\odot}$, $\theta = 0°$, and $\phi = 180°$. The domain covers $-87.5° \le \theta \le 87.5°$; $0° \le \phi \le 360°$; $18\ \mathrm{R}_{\odot} \le r \le 345\ \mathrm{R}_{\odot}$. An open boundary condition at both $\theta = 87.5°$ and $\theta = -87.5°$ is used, so that there are no reflective disturbances. A constant grid size of $\Delta r = 3\ \mathrm{R}_{\odot}$, $\Delta\theta = 5°$, and $\Delta\phi = 5°$ is used, which results in $110 \times 36 \times 72$ grid sets.

3.3.1. Simulation Results

For the purpose of adding a CME perturbation into the simulation, a pressure pulse is used as a proxy. The observed CME information such as the CME source location, onset time, and speed are used to construct the pressure pulse. The source location of the solar flare associated with the CME is used as the center of the CME perturbation, if both STEREO-A/B coronal imagers were not available at the same time. Note that STEREO-B has lost contact since September 2015. Coronal imagers of STEREO/*Cor2* (called *Cor2a* is hereafter) are used to estimate the CME propagation speeds [V_{CME}] for this study. Both CME04 and

CME06 are halo CMEs. The size of a halo CME is less than 120° in the θ- and ϕ-directions (*e.g.* Wood *et al.*, 2017).

To initiate the CME, a pressure (velocity + density) pulse of a Gaussian shape is imposed at the inner boundary of the computational domain ($r = 18\ \mathrm{R}_\odot$). Two pressure pulses were added to simulate the evolution of both CME04 and CME06. The values of V_{CME04} ($886\ \mathrm{km\,s^{-1}}$) and V_{CME06} ($1368\ \mathrm{km\,s^{-1}}$) estimated in the previous section used as the initial CME speeds at $18\ \mathrm{R}_\odot$. The duration [δt] of the pressure pulse is a free parameter to tune the ejecta time to match the arrival time of the CME-driven shock with observations and the solar wind profile at Earth. Table 1 lists the detailed information about source location, eruption time, and propagation speed of these two CMEs. We tuned the δt of the pressure pulses to match the shock-arrival time (SAT) at *Wind* (or ≈ 1 AU). The value of δt was three hours for both CME04 and CME06 to match the shock-arrival time (SAT) at the *Wind* spacecraft.

Figure 8 shows the evolution of CME04 and CME06 from the Sun to the Earth and their interaction. Figure 8 shows scatter plots of the simulated time series of solar wind velocity profiles at a plane 7.5° above the solar Equator (or 7.5°N). An undisturbed background solar wind profile (at 12:37 UT, 04 September 2017) is shown in Figure 8a. Figures 8b (at 00:36 UT on 05 September) and 8e (at 15:29 UT on 06 September) show that CME04 and CME06 were ejected from the inner boundary. Figure 8f (at 22:31 UT on 06 September) and Figure 8h (at 20:28 UT on 07 September) show the front edges of CME04 and CME06 that encountered the Earth. Figures 8g (at 12:31 UT on 07 September), 8h, and 8i show the interaction between CME04 and CME06. Figure 8g shows that CME06 encountered the rear part of CME04. CME06 and CME04 merged at 12:35 UT on 08 September (see Figure 8i). Simulation results also show clearly that a high-speed structure (or a CME and its driven shock) has passed the Earth on 06 and 07 September 2017, and the center of both CME04 and CME06 were off the Sun–Earth line by many degrees. The east boundaries of CME04 and CME06 encountered the Earth.

In-situ observations show that the duration of Sheath06 (≈ 21 hours) was $\approx 75\%$ longer than that of a typical sheath. Note that the typical duration of a sheath is ≈ 12 hours (*e.g.* Wu and Lepping, 2016). The encountered part of CME04 was far away from CME04's center. This is the main reason for the unusually long duration of Sheath06. Here, we demonstrate that the 3D MHD simulation can be a useful tool in identifying the driver for an IP shock, and to explain an unusually long duration of sheath06.

3.3.2. Comparison of in-Situ Observation Versus Simulation Results

Validation of simulation results is one of the important procedures for G3DMHD simulation. Comparing simulation results with *in-situ* observations of solar wind plasma and field parameters is one of the ways to validate G3DMHD simulations. Figure 9a shows a comparison between observations (from *Wind* in red-dotted curves) and the simulation of background solar wind (in black-solid curves) during 05 September – 01 October. The two vertical blue-dotted lines indicate IP shocks' arrival time (SAT) at *Wind*, which is located at $\approx 212.84\ \mathrm{R}_\odot$. The labels "Shock06" and "Shock07" indicate that the IP shocks arrived at the *Wind* spacecraft on 06 September 2017 and 07 September 2017, respectively. No IP shock was formed in the simulation, because no CME perturbation was added into the simulation. Correlation coefficients (ccs) for simulation *versus* observations are 0.67, 0.52, 0.33, and 0.37 for velocity [V_r], density [N_p], temperature [T_p], and magnetic field [B], respectively.

Figure 9b shows the comparison between observations and simulations with two CMEs' perturbations during 05 – 09 September. The values of ccs for simulation *versus* observation are 0.84, 0.79, 0.73, and -0.02 for V, N_p, T_p, and B, respectively. Simulated solar wind

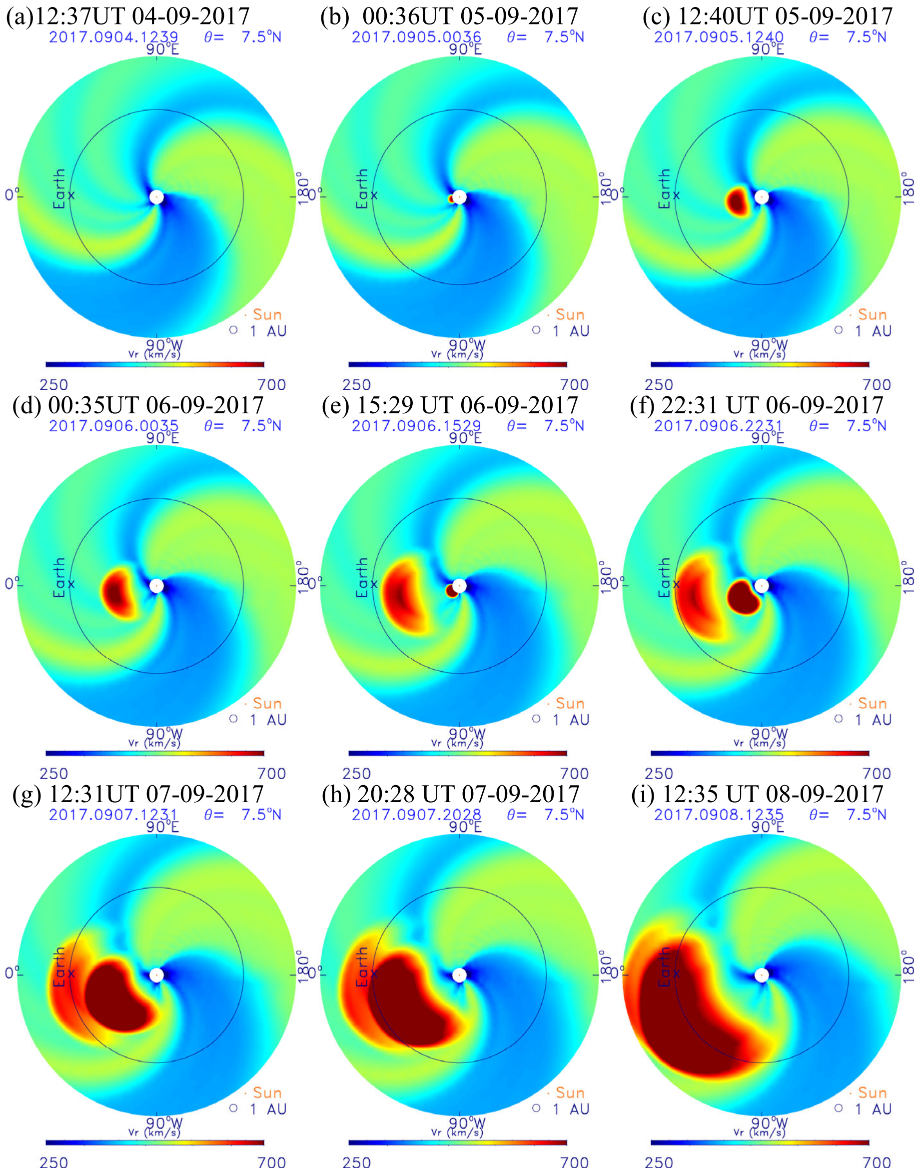

Figure 8 Temporal profile of simulated solar wind velocity in the plane of 7.5°N of the solar Equator during 04 – 08 September 2017 by using velocity formula $Vr = 150 + 500 f_s^{-0.4}$ for velocity variation at 18 $R_\odot$. (**a**): Undisturbed solar wind. (**b**) and (**e**): CME04 and CME06 ejected from 18 $R_\odot$. (**f**) and (**h**): IP Shock06 and Shock07 arrived at the Earth.

speed [V_{G3DMHD}] at the downstream of the IP shocks (V_{peak}: peak of solar wind speed) is well correlated with the observations for both Shock06 and Shock07. The simulated $N_{\mathrm{p_{peak}}}$ (peak of solar wind density) at the downstream of Shock06 and Shock07 are also reasonably well correlated with observations. $B_{\text{peak-G3DMHD}}$ (peak of IMF in the simulation) at Shock06 downstream is also reasonably well correlated, but $B_{\text{peak-G3DMHD}}$ was too low for Shock07.

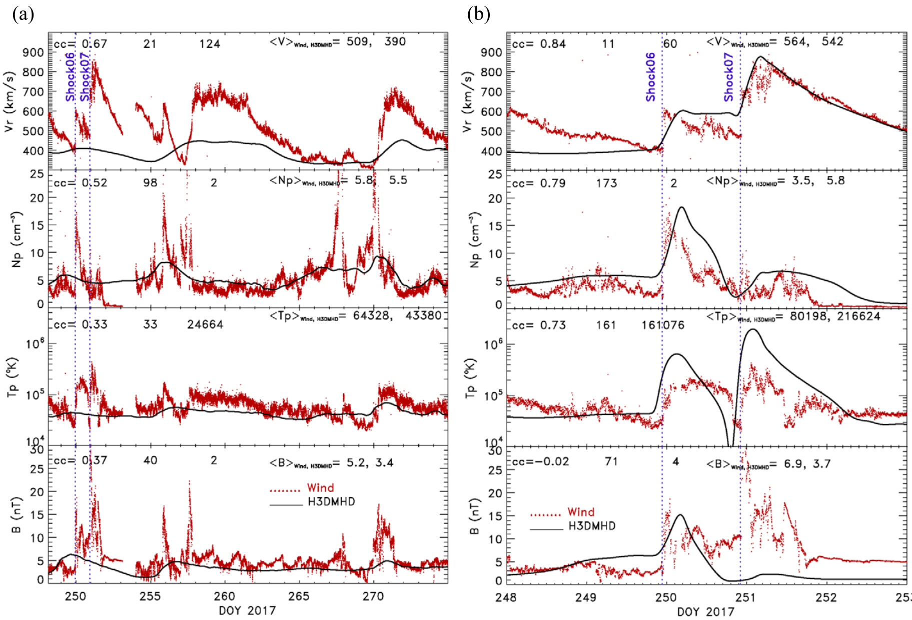

Figure 9 *In-situ* (*red-dotted curves*) and G3DMHD (*black-solid curves*) solar wind in September 2017. (**a**) Comparison of undisturbed G3DMHD background solar wind with observation (*Wind*) during 05 September – 01 October 2017. (**b**) Comparison of disturbed G3DMHD solar wind with observation of during 05 – 09 September 2017: simulated CME04 and CME06 were ejected at 18 $R_\odot$. Shock06 and Shock07 were marked by *two vertical blue-dotted lines*.

Our MHD simulation results correspond reasonably well with the observations in a number of areas: i) SAT at *Wind*; ii) solar wind speed upstream of Shock06; iii) solar wind speed downstream of Shock06 and Shock07, and the temporal profile of the solar wind speed after Shock07 encountered *Wind* matched perfectly with observation for approximately two days (DOY 251 – 253); iv) solar wind density downstream of Shock06 and Shock07; v) IMF B downstream of Shock06; and vi) solar wind temperature profile upstream of Shock06, and in the period of 05 – 09 September.

The average propagation speeds (from 18 $R_\odot$ to 1 AU) for $\langle V_{\text{Shock06}}\rangle$ and $\langle V_{\text{Shock07}}\rangle$ were 792 $\mathrm{km\,s^{-1}}$ and 1159 $\mathrm{km\,s^{-1}}$, respectively (see Table 1). The differences between $\langle V_{\text{shock}}\rangle$ and V_{CME} are ≈ 76 and 209 $\mathrm{km\,s^{-1}}$ for the events of CME04–Shock06 and CME06–Shock07, respectively. The difference between $V_{\text{CME@18R}_\odot}$ and $\langle V_{\text{Shock}}\rangle$ is one of the main causes for the error in the estimation of the SAT.

The values of Δt_{Error} for the CME04–Shock06 [$\Delta t_{\text{Error.CME04-Shock06}}$] and CME06–Shock07 [$t_{\text{Error.CME06-Shock07}}$] events are 4.05 and 4.97 hours, respectively. The errors ($\equiv \Delta t_{\text{Error}}/\Delta t_{\text{Shock-CME@18R}_\odot} \times 100\%$) are 8.5% and 15%, respectively. (Note that the large error of $\Delta t_{\text{Shock07-CME06}}$ is caused by a small value of $\Delta t_{\text{Shock07-CME06@18R}_\odot}$; see Table 1.) However, the errors for both events are smaller than $\approx 15\%$, which is not large. Hence, the coronagraph technique can be a viable tool to estimate the initial speed of the CME.

The large error of $\Delta t_{\text{Error.CME06-Shock07}}$ may be caused by the disturbed background solar wind of the CME06–Shock07 event. Note that the difference in the eruption times of CME04 and CME06 was less than two days, and V_{CME06} was $\approx 60\%$ faster than V_{CME04}. The leading edge of CME06–Shock07 interacted with the rear part of CME04–Shock06 (or the downstream of Shock06) while CME06–Shock07 was on its way to the Earth. Note that CME06 may be slowing down or speeding up while it was on its way to the Earth. In this study, CME04–Shock06 and CME06–Shock07 were slowing down by factors of 8.5% and 15%, respectively. The speed difference between $\langle V_{\mathrm{CME}} \rangle$ and $\langle V_{\mathrm{Shock}} \rangle$ may be caused by the interaction between different kinds of solar wind structures, *e.g.* the background (or non-disturbed) solar wind and the disturbed solar wind (*i.e.* a CME and its driven shock). Previous studies suggest that a fast CME generally will be decelerated on its way to the Earth, but a slow CME will be accelerated (*e.g.* Gopalswamy *et al.*, 2000). Both CME04 and CME06 are in the category of the fast CMEs. Therefore, they were most likely slowing down when they arrived at 1 AU. These results are consistent with previous studies (*e.g.* Liou *et al.*, 2014; Gopalswamy, 2016). Note that V_{CME06} was 1.58 times V_{CME04} at $\approx 18\ \mathrm{R}_{\odot}$ and V_{Shock07} was 1.46 times V_{Shock06} at ≈ 1 AU. Hence, this suggests that, in general, a CME with a higher propagating speed will decelerate faster than a CME with lower propagating speed. Figure 9b shows clearly that the solar wind density in the region between Shock06 and Shock07 was higher than that at the upstream of Shock06. This result is in contrast to the general assumption that the preceding event paves the way for the later event (arriving earlier) by removing solar wind density (*e.g.* Liu *et al.*, 2014).

4. Summary and Conclusions

We have studied two Sun–Earth-directed ICME events that occurred in the early September 2017 (04 and 06 September) time-frame. What made the two events special is that they are "catch-up" CME events: V_{CME04} ($= 866\ \mathrm{km\,s^{-1}}$) is slower than the V_{CME06} ($= 1387\ \mathrm{km\,s^{-1}}$). These initial CME speeds were estimated with time series of coronagraph images and validated by MHD simulations. The estimated (Sun–Earth) shock-arrival time (SAT) at the Earth is 43.47 hours. It took ≈ 47.52 hours for Shock07 to arrive at the Earth. The error was only 8.5%.

V_{CME06} was almost 50% faster than V_{CME04}. The *in-situ* solar wind data and the Dst-index show that the $\mathrm{Dst_{min}}$ value of Storm08 was caused by the southward IMF B_z of MC07, as expected. MC07 was associated with CME04. The duration of MC07 [Δt_{MC07}] is rather short: $\approx$ five hours ($\Delta t_{\mathrm{MC07}} \approx$ five hours). The short Δt_{MC07} may be caused by the interaction between MC07 and Shock07, or the source location of CME04 was not at or near the longitude of the Sun–Earth line. In addition, the sharp B_z drop in the middle of MC07 may also be caused by the interaction of the MC07–Shock07 (IP shock compression), *i.e.* MC07 B_z was compressed by Shock07 from behind. Storm07 was a complicated event, because it was caused by the combination of two interplanetary structures. One may categorize it as a "sheath storm" that was caused by the southward part of B_z in the sheath region of Shock07.

The source locations of CME04 and CME06 were S10W11 and S10W33, respectively. The center of Shock07/CME06 was farther away from the Earth than for the center of Shock06/CME04 complex. Therefore, Shock07/CME06 did not induce bigger geomagnetic activity than Shock06/CME04. These results also show that the location (*i.e.* latitude and longitude) of the solar disturbance (*e.g.* CME) is another important factor in space-weather prediction. In this study, we used V_{CME} only to estimate the SAT for two CME events in September 2017. The results are quite good. This technique was employed previously by Wu *et al.* (2016a), who studied the first severe geomagnetic storm (St. Patrick Day's Storm 2015) in Solar Cycle 24. More such case studies are required to make sure this technique is appropriate for all events.

In this study, we examined the evolution of two Sun–Earth-directed ICME events that occurred on 04 and 06 September 2017. We also investigated the associated geomagnetic activity after these two events encountered the Earth. The following phenomena were found:

i) the CME speed determined at 18 $R_\odot$ using coronagraph images can be a good estimator for predicting the ICME-driven shock's arrival time at the Earth when there is no pre-event; ii) a relatively severe geomagnetic storm can be caused by the interaction between the Earth's magnetosphere and a system in which a MC is simultaneously interacting with an impinging IP shock at its rear (note: this is a rare event); and iii) the intensity of a geomagnetic storm will likely be stronger for an event associated with ICME–ICME interaction than by a geomagnetic event caused by only a single ICME.

In order to settle the argument about the use of V_{CME}, which was measured from the plane-of-the-sky, a three-dimensional MHD simulation is performed to address this issue by providing a panoramic view of the entire process, which is not available from the observations. The simulation demonstrates a good match between the predicted and observed shock-arrival times, suggesting that V_{CME} measured at 18 $R_\odot$ with the SAT is reasonably accurate.

Acknowledgements All data used in this study are obtained from the public domain. We thank the *Wind* PI teams and the National Space Science Data Center at NASA/Goddard Space Flight Center, for providing the solar wind plasma and magnetic-field data. The work of C.C. Wu was supported partially by the Chief of Naval Research and the NASA LWS 80HQTR18T0023 and HSWO2R17-0005 grants to the Naval Research Laboratory. The work of K. Liou was supported by the NSF grant 1743118 to the Johns Hopkins University Applied Physics Laboratory.

Disclosure of Potential Conflicts of Interest The authors declare that there is no conflict of interest for publishing this research results in Solar Physics.

Publisher's Note Springer Nature remains neutral with regard to jurisdictional claims in published maps and institutional affiliations.

References

Bothmer, V., Schwenn, R.: 1996, Signatures of fast CMEs in interplanetary space. *Adv. Space Res.* **17**, 319. DOI.

Cane, H.V., Richardson, I.G.: 2003, Interplanetary coronal mass ejections in the near-Earth solar wind during 1996 – 2002. *J. Geophys. Res.* **108**, 1156. DOI.

Chashei, I.V., Tyul'bashev, S.A., Shishov, V.I., Subaev, I.A.: 2018, Coronal mass ejections in September 2017 from monitoring of interplanetary scintillations with the large phase array of the Lebedev Institute of Physics. *Astron. Rep.* **62**, 346. DOI.

Collier, M.R., Lepping, R.P., Berdichevsky, D.B.: 2007, A statistical study of interplanetary shocks and pressure pulses internal to magnetic clouds. *J. Geophys. Res.* **112**, A06102. DOI.

Dryer, M.: 1994, Interplanetary studies: Propagation of disturbances between the Sun and the magnetosphere. *Space Sci. Rev.* **67**, 363. DOI.

Echer, E., Gonzalez, W.D.: 2004, Geoeffectiveness of interplanetary shocks magnetic clouds, sector boundary crossings and their combined occurrence. *Geophys. Res. Lett.* **31**, L09808. DOI.

Fry, C.D., Sun, W., Deehr, C.S., Dryer, M., Smith, Z., Akasofu, S.-I., Tokumaru, M. Kojima, M.: 2001, Improvements to the HAF solar wind model for space weather predictions. *J. Geophys. Res.* **106**(A10), 20985. DOI.

Gopalswamy, N.A.: 2016, History and development of coronal mass ejections as a key player in solar terrestrial relationship. *Geosci. Lett.* **3**, 8, 18 pp. DOI.

Gopalswamy, N.A., Lara, A., Lepping, R.P., Kaiser, M.L., Berdichevsky, D.B., St. Cyr, O.C.: 2000, Interplanetary acceleration of coronal mass ejections. *Geophys. Res. Lett.* **27**, 145. DOI.

Gopalswamy, N., Lara, A., Yashiro, S., Kaiser, M.L., Howard, R.A.: 2001, Predicting the 1-AU arrival of coronal mass ejections. *J. Geophys. Res.* **106**(A12), 29209. DOI.

Gosling, J.T.: 1990, Coronal mass ejections and magnetic flux ropes in interplanetary space. In: *Physics of Magnetic Flux Ropes (A92-31201 12-75)*, Am. Geophys. Union, Washington, 343. DOI.

Gosling, J.T., Hilder, E., MacQueen, R.M., Munro, R.H., Poland, A.I., Ross, C.L.: 1975, Direct observations of a flare related coronal and solar wind disturbance. *Solar Phys.* **40**, 439. DOI.

Gonzalez, W.D., Joselyn, J.A., Kamide, Y., Kroehl, H.W., Rostoker, G., Tsurutani, B.T., Vayliuma, V.M.: 1994, What is a geomagnetic storm? *J. Geophys. Res.* **99**, 5771. DOI.

Guo, J. Dumbović, M. Wimmer-Schweingruber, R.F., Temmer, M., Lohf, H., Wang, Y., *et al.*: 2018, *Space Weather* **16**(8), 1156. DOI.

Hakamada, K., Akasofu, S.-I.: 1982, Simulation of three-dimensional solar wind disturbances and resulting geomagnetic storms. *Space Sci. Rev.* **31**, 3.

Han, S.M., Wu, S.T., Dryer, M.: 1988, A three-dimensional, time-dependent numerical modeling of supersonic, super-Alfvénic MHD flow. *Comput. Fluids* **16**, 81 (ISSN 0045-7930)

Huttunen, K.E.J., Schwenn, R., Bothmer, V., Koskinen, H.E.J.: 2005, Properties and geoeffectiveness of magnetic clouds in the rising, maximum and early declining phases of solar cycle 23. *Ann. Geophys.* **23**(2), 625. DOI.

Kamide, Y., Yokoyama, N., Gonzalez, W., Tsurutani, B.T., Daglis, I.A., Brekke, A., Masuda, S.: 1998, Two-step development of geomagnetic storms. *J. Geophys. Res.* **103**, 6917. DOI.

Lax, P.D., Wendroff, B.: 1960, Systems of conservation laws. *Comm. Pure Appl. Math.* **13**, 217.

Lepping, R.P., Jones, J.A., Burlaga, L.F.: 1990, Magnetic field structure of interplanetary magnetic clouds at 1 AU. *J. Geophys. Res.* **95**(A8), 11957. DOI.

Lepping, R.P., Wu, C.-C., Berdichevsky, D.B.: 2005, Automatic identification of magnetic clouds and cloud-like regions at 1 AU: Occurrence rate and other properties. *Ann. Geophys.* **23**, 2687. DOI.

Lepping, R.P., Berdichevsky, D.B., Wu, C.-C., Szabo, A., Narock, T., Mariani, F., Lazarus, A.J., Quivers, A.J.: 2006, A summary of WIND magnetic clouds for years 1995 – 2003: Model-fitted parameters, associated errors and classifications. *Ann. Geophys.* **24**, 215. DOI.

Liou, K., Wu, C.-C., Dryer, M., Wu, S.T., Nathan, R., Plunkett, S., Simpson, L., Fry, C.D., Schenk, K.: 2014, Global simulation of extremely fast coronal mass ejection on 23 July 2012. *J. Atmos. Solar-Terr. Phys.* **121**, 32. DOI.

Liu, Y.D., Luhmann, J.G., Kajdič, P., Kilpua, E.K.J., Lugaz, N., Nitta, V., Möstl, C., Lavraud, B., Bale, S.D., Farrugia, C.J., Galvin, A.B.: 2014, Observations of an extreme storm in interplanetary space caused by successive coronal mass ejections. *Nat. Commun.* **5**, 3481. DOI.

McAllister, A.H., Crooker, N.U.: 1997, Coronal mass ejections, corotating interaction regions, and geomagnetic storms. In: Crooker, N., Joselyn, J.A., Feynman, J. (eds.) *Coronal Mass Ejections*, *Geophys. Monogr. Ser.* **99**, Am. Geophys. Union, Washington, 279. DOI.

Owens, M., Cargill, P.: 2004, Predictions of the arrival time of coronal mass ejections at 1 AU: An analysis of the causes of errors. *Ann. Geophys.* **22**(2), 661. DOI.

Richardson, I.G., Cane, H.: 2011, Geoeffectiveness (Dst and Kp) of interplanetary coronal mass ejections during 1995 – 2009 and implications for storm forecasting. *Space Weather* **9**, S07005. DOI.

Schwenn, R., dal Lago, A., Huttunen, E., Gonzalez, W.D.: 2005, The association of coronal mass ejections with their effects near the Earth. *Ann. Geophys.* **23**(3), 1033. DOI.

Sheeley, N.R. Jr., Howard, R.A., Michel, D.J., Koomen, M.J., Schwenn, R., Muehlhaeuser, K.H., Rosenbauer, H.: 1985, Coronal mass ejections and interplanetary shocks. *J. Geophys. Res.* **90**, 163. DOI.

Sugiura, M.: 1953, The solar diurnal variation in the amplitude of sudden commencements of magnetic storms at the geomagnetic equator. *J. Geophys. Res.* **58**, 558. DOI.

Tsurutani, B.T., Gonzalez, W.D.: 1997, In: Tsurutani, B.T., Gonzalez, W.D., Kamide, Y. (eds.) *The Interplanetary Causes of Magnetic Storms: A Review*, *Geophys. Monogr. Ser.* **98**, Am. Geophys. Union, Washington, 77. DOI.

Tsurutani, B.T., Smith, E.J., Gonzalez, W.D., Tang, F., Akasofu, S.I.: 1988, Origin of interplanetary southward magnetic fields responsible for major magnetic storms near solar maximum (1978 – 1979). *J. Geophys. Res.* **93**, 8517. DOI.

Vršnak, B., Zic, T., Falkenberg, T.V., Möstl, C., Vennerstrom, S., Vrbanec, D.: 2010, The role of aerodynamic drag in propagation of interplanetary coronal mass ejections. *Astron. Astrophys.* **512**, A43. DOI.

Wood, B.E., Wu, C.-C., Howard, R.A., Socker, D.G., Rouillard, A.P.: 2011, Empirical reconstruction and numerical modeling of the first geoeffective coronal mass ejection of solar cycle 24. *Astrophys. J.* **729**, 70. DOI.

Wood, B.E., Wu, C.-C., Rouillard, A.P., Howard, R.A., Socker, D.G.: 2012, A coronal hole's effects on CME shock morphology in the inner heliosphere. *Astrophys. J.* **755**, 43. DOI.

Wood, B.E., Wu, C.-C., Lepping, R.P., Nieves-Chinchilla, T., Howard, R.A., Linton, M.G., Socker, D.G.: 2017, A STEREO survey of magnetic cloud coronal mass ejections observed at Earth in 2008 – 2012. *Astrophys. J. Suppl.* **229**(2), 29, 26 pp. DOI.

Wu, C.-C., Lepping, R.P.: 2002a, Effects of magnetic clouds on the occurrence of geomagnetic storms: the first 4 years of wind. *J. Geophys. Res.* **107**(A10), 1314. DOI.

Wu, C.-C., Lepping, R.P.: 2002b, Effect of solar wind velocity on magnetic cloud-associated magnetic storm intensity. *J. Geophys. Res.* **107**(A11), 1346. DOI.

Wu, C.-C., Lepping, R.P.: 2007, Comparison of the characteristics of magnetic clouds and magnetic cloud-like structures for the events of 1995 – 2003. *Solar Phys.* **242**, 159. DOI. ADS.

Wu, C.-C., Lepping, R.P.: 2008, Geomagnetic activity associated with magnetic clouds, magnetic cloud-like structures and interplanetary shocks for the period 1995 – 2003. *Adv. Space Res.* **41**, 335. DOI. ADS.

Wu, C.-C., Lepping, R.P.: 2011, Statistical comparison of magnetic clouds with interplanetary coronal mass ejections for solar cycle 23. *Solar Phys.* **269**, 141. DOI. ADS.

Wu, C.-C., Lepping, R.P.: 2016, Relationships among geomagnetic storms, interplanetary shocks, magnetic clouds, and sunspot number during 1995 – 2012. *Solar Phys.* **291**, 265. DOI. ADS.

Wu, C.C., Lepping, R.P., Gopalswamy, N.: 2006, Relationships among magnetic clouds, CMES, and geomagnetic storms. *Solar Phys.* **239**, 449. DOI. ADS.

Wu, C.-C., Fry, C.D., Wu, S.T., Dryer, M., Liou, K.: 2007a, Three-dimensional global simulation of ICME propagation from the Sun to the heliosphere: 12 May 1997 solar event. *J. Geophys. Res.* **112**, A09104, DOI.

Wu, C.-C., Fry, C.D., Wu, S.T., Dryer, M., Thompson, B., Liou, K., Feng, X.S.: 2007b, Three-dimensional global simulation of multiple ICMEs' interaction and propagation from the Sun to the heliosphere following the 25 – 28 October 2003 solar events, coronal mass ejections. *Adv. Space Res.* **40**, 1827. DOI.

Wu, C.-C., Dryer, M., Wu, S.T., Wood, B., Fry, C.D., Liou, K., Plunkett, S.: 2011, Global three-dimensional simulation of the interplanetary evolution of the observed geoeffective CME during the epoch August 1 – 4, 2010. *J. Geophys. Res.* **116**, A12103 13 pp. DOI.

Wu, C.-C., Gopalswamy, N., Lepping, R.P., Yashiro, S.: 2013, Characteristics of magnetic clouds/interplanetary coronal mass ejections which caused intense geomagnetic storms. *Terr. Atmos. Ocean. Sci.* **24**, 233. DOI.

Wu, C.-C., Liou, K., Lepping, R.P., Hutting, L., Plunkett, S., Howard, R.A., Socker, D.: 2016a, The first super geomagnetic storm of solar cycle 24: "The St. Patrick's day event (17 March 2015)". *Earth Planets Space* **68**(1), 151, 12 pp. DOI.

Wu, C.-C., Liou, K., Vourlidas, A., Plunkett, S., Dryer, M., Wu, S.T., Mewaldt, R.A.: 2016b, Global magnetohydrodynamic simulation of the March 15, 2013 coronal mass ejection event – Interpretation of the 30 – 80 MeV proton flux. *J. Geophys. Res.* **121**(1), 56. DOI.

Wu, C.-C., Liou, K., Vourlidas, A., Plunkett, S., Dryer, M., Wu, S.T., Socker, D., Wood, B.E., Hutting, L., Howard, R.: 2016c, Numerical simulation of multiple CME-driven shocks in the month of 2011 September. *J. Geophys. Res.* **121**, 1839. DOI.

Wu, C.-C., Liou, K., Lepping, R.P., Vourlidas, A., Plunkett, S., Socker, D., Wu, S.T.: 2017, Observation of an extremely large-density heliospheric plasma sheet compressed by an interplanetary shock at 1 AU. *Solar Phys.* **292**, 109. DOI.

Wu, C.-C., Liou, K., Plunkett, S., Socker, D., Wang, Y.M., Wood, B.E., Wu, S.T., Dryer, M., Kung, C.: 2019, Modeling inner boundary values at 18 solar radii during solar quiet time for global three-dimensional time-dependent magnetohydrodynamic numerical simulation. *J. Atmos. Solar-Terr. Phys.* (Submitted). arXiv.

Yashiro, S., Gopalswamy, N., Cliver, E.W., Reames, D.V., Kaiser, M.L., Howard, R.A.: 2004, Association of coronal mass ejections and type II radio bursts with impulsive solar energetic particle events, the solar-B mission and the forefront of solar physics. In: Sakurai, T., Sekii, T. (eds.) *Proceedings of the Fifth Solar-B Science Meeting Held 12 – 14 November, 2003 in Roppongi, Tokyo, Japan*, *ASP Conference Series* **325**, Astron. Soc. Pacific, San Francisco, 401. ADS.

Zhang, J., Richardson, I.G., Webb, D.F., Gopalswamy, N., Huttunen, E., Kasper, J., Nitta, N., Poomvises, W., Thompson, B.J., Wu, C.-C., Yashiro, S., Zhukov, Z.: 2007, Solar and interplanetary sources of major geomagnetic storms (Dst < -100 nT) during 1996 – 2005. *J. Geophys. Res.* **112**, A10102. DOI.